Lessons learned from initial Sentinel-3A maneuver operations

By Daniel AGUILAR TABOADA[1)], Pier Luigi RIGHETTI[2)] and Rami HOUDROGE[3)]

[1)]*CLC Space at EUMETSAT, Germany*
[2)]*EUMETSAT, Germany*
[3)]*Serco at EUMETSAT, Germany*

Sentinel-3A, first of the Sentinel-3 fleet of the European Commission's Copernicus programme, was launched from Plesetsk Cosmodrome on a Rockot launcher on 16 February 2016. Sentinel-3 satellites fly around the Earth on a Sun-synchronous orbit with a repeat cycle of 27 days and cycle length of 385 orbits with an orbit control requirements of ±1 km with respect to the reference ground track. In order to maintain the orbit within prescribed requirements, Sentinel-3 satellites are equipped with two sets of four 1-Newton monopropellant hydrazine thrusters. One out-of-plane station keeping maneuver is needed every three to four months and one in-plane station keeping maneuver is needed every two to eight weeks depending on the level of solar activity. Regarding the out-of-plane maneuvers that have been already performed, it has been observed that the observed pulse distribution among the thrusters was different than predicted which induced (a) different maneuver duration and (b) misalignment in main thrust direction. (a) caused reduced performances in orbit determination solution due mainly to delta-V centroid displacement and (b) caused relatively early need of touch-up in-plane maneuver. These prediction errors in pulse distribution can be due to inaccurate knowledge of centre-of-mass, thruster alignments or positions as well as force generated by each thruster. If centre-of-mass is considered the driver for the observed differences, its displacement with respect to on-ground knowledge can be estimated for each out-of-plane maneuver by checking the unload control torque or the difference in pulses distribution observed in satellite telemetry. A systematic displacement of the centre-of-mass is observed and its evolution might be explained by an eccentric rotation of the solar panel with respect to its centre-of-mass. Pulses distribution is estimated for last out-of-plane maneuver accounting for past knowledge of centre-of-mass displacements showing positive results.

Key Words: Sentinel-3A, maneuver, pulses distribution, centre-of-mass, orbit determination

Nomenclature

$\vec{\boldsymbol{\tau}}$	:	torque
$\vec{\boldsymbol{r}}$	:	position
$\vec{\boldsymbol{f}}$	:	force
$\boldsymbol{p}$	:	number of pulses
Subscripts		
d	:	drag
g	:	gravitational field
s	:	solar radiation pressure
i	:	internal forces
t	:	thruster
m	:	centre-of-mass
Superscripts		
O	:	spacecraft body frame origin

1. Introduction

Sentinel-3A, first of the Sentinel-3 fleet of the European Commission's Copernicus programme, was launched from Plesetsk Cosmodrome on a Rockot launcher on 16th February 2016. Sentinel-3 satellites fly around the Earth on a Sun-synchronous orbit with a repeat cycle of 27 days and cycle length of 385 orbits with an orbit control requirements of ±1 km with respect to the reference ground track. In order to maintain the orbit within prescribed requirements, Sentinel-3 satellites are equipped with two sets of four 1-Newton monopropellant hydrazine thrusters. One out-of-plane station keeping maneuver of around 2m/s is needed every three to four months and one in-plane station keeping maneuver of around 4 to 20mm/s is needed every two to eight weeks depending on the level of solar activity.

Thruster set#1 is used for out-of-plane maneuvers providing an almost ideal thrust direction. It is located on the $-X_S$ panel of the platform. Figure 1 describes the satellite axes convention.

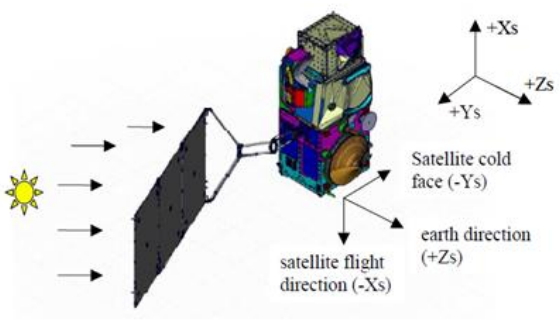

Fig. 1. Sentinel-3A satellite

The thrusters are commanded in off modulation in order to allow wheels unloading control during the boost with an unload cycle duration of 12.5s, a pulse duration of 0.125s, a minimum duty cycle of 0.2 (20 pulses per thruster during an unload cycle) and a maximum allowed duty cycle that goes from 0.77 during first unload cycle (to reduce risk of wheel saturation) to a maximum of 0.92 from the eighth unload cycle. Figure 2 shows the evolution of the minimum and maximum duty cycles as function of the unload cycle.

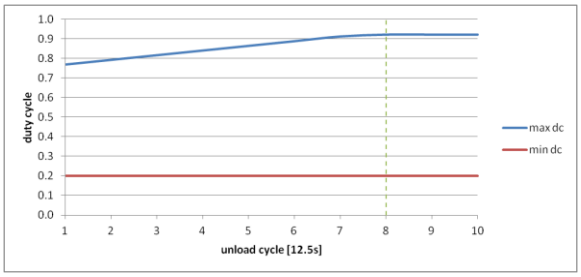

Fig. 2. Maximum and minimum duty cycle profile

On ground, thrusters duty cycles are estimated at each unload cycle such that the total torque generated by the four thrusters is nullified. On board, the first unload cycle is implemented exactly as estimated on ground. As of the second cycle, the on-board software re-computes the thrusters duty cycles accounting for the observed torque generated during the previous unload cycle.

2. Prediction versus reality

Differences in pulses distribution among thrusters have been observed between on-ground estimations and actual realization by the satellite. Tables 1 and 2 show the predicted and actually implemented pulses per thruster for all out-of-plane maneuvers with a size greater than 1.2m/s.

Man#	Predicted Pulses				
	Thr#1	Thr#2	Thr#3	Thr#4	Total
1	1839	1879	1985	1943	7646
2	2700	2761	2916	2854	11231
3	3508	3588	3788	3708	14592
4	4587	4694	4959	4852	19092
5	4702	4812	5082	4972	19568

Table 1. Predicted pulses

Man#	Implemented Pulses				
	Thr#1	Thr#2	Thr#3	Thr#4	Total
1	1936	1672	1933	2107	7648
2	2808	2386	2801	3236	11231
3	3731	3157	3695	4010	14593
4	4948	4188	4886	5071	19093
5	4953	4204	4938	5475	19570

Table 2. Implemented pulses

These differences result in both different maneuver duration and thrust direction as illustrated in Tables 3 and 4.

Man#	Maneuver duration		
	Predicted	Actual	Difference
1	277.125s	294.875s	6.4%
2	403.750s	448.000s	11.0%
3	521.500s	554.250s	6.3%
4	680.875s	698.625s	2.6%
5	697.250s	753.250s	8.0%

Table 3. Maneuver durations

Man#	Delta-V Differences [mm/s]		
	Radial	Along-track	Cross-track
1	-2.3	3.4	-0.01
2	-5.5	6.3	-0.04
3	-4.3	6.7	-0.03
4	-2.9	7.3	-0.02
5	-7.1	9.3	-0.04

Table 4. delta-V difference

The differences in maneuver durations cause a displacement of the maneuver centroid generating a small change in right ascension of the ascending node that in turns causes poor performances in orbit determination solution. This has been mitigated by feeding orbit determination software with maneuver duration as observed in telemetry.

The differences in radial and along-track directions of delta-V cause relatively early need of in-plane maneuver noting that reported error is comparable with nominal size of in-plane maneuver. This has been mitigated by accounting for error margins in the definition of the main thrust direction and by extrapolating observed difference in maneuver N in the preparation of maneuver N+1.

The differences in pulse distribution can be due to inaccurate knowledge of centre-of-mass, thruster alignments or positions as well as forces generated by each thruster.

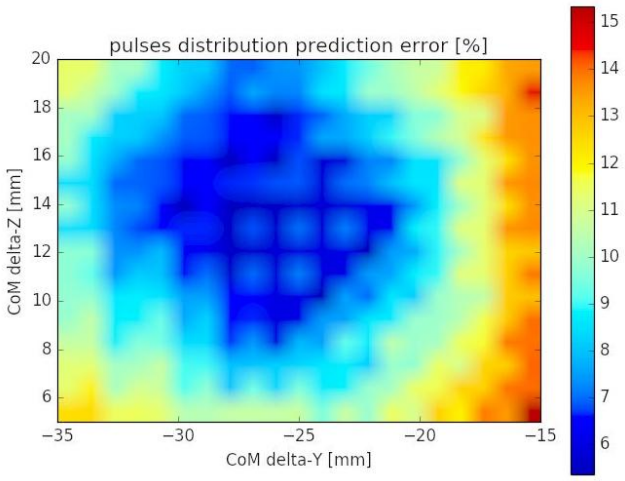

Fig. 3. Pulses distribution prediction error for OOP maneuver performed on 2017-03-15

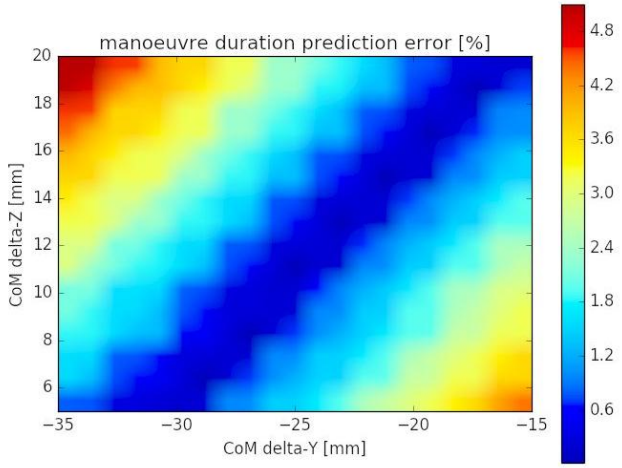

Fig. 4. Maneuver duration prediction error for OOP maneuver performed on 2017-03-15

Figures 3 and 4 illustrate how the pulses distribution and maneuver duration error vary as function of the centre-of-mass displacement in Ys and Zs direction (as main thrust direction is along in Xs direction); it can be observed that a common displacement reduces strongly both errors.

3. Centre-of-mass estimation

The perturbing torque experienced by the satellite can be expressed as:

$$\vec{\tau} = \vec{\tau}_d + \vec{\tau}_g + \vec{\tau}_s + \vec{\tau}_i \quad (1)$$

where $\vec{\tau}_d$ is the torque due to atmospheric drag force, $\vec{\tau}_g$ is the torque due to gravitational force, $\vec{\tau}_s$ is the torque due to solar radiation pressure and $\vec{\tau}_i$ is the torque due to internal forces such as internal moving mechanisms.

Figure 4 shows unload control torque reported in satellite telemetry. It can be observed that thrusters are the main perturbing force during maneuvers.

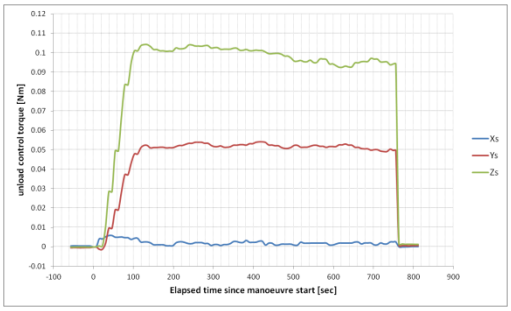

Fig. 5. Unload control torque profile during last OOP maneuver performed on 2017-03-15

We can assume:

$$\vec{\tau} \approx \vec{\tau}_i \quad (2)$$

$$\vec{\tau}_i \approx \sum_{t=1}^{t=4} \vec{\tau}_t \quad (3)$$

where $\vec{\tau}_t$ is the torque generated by each thruster.

Equation (4) describes the torque generated by the thrusters as function of thrusters' positions with respect to the centre-of-mass and forces.

$$\sum_{t=1}^{t=4} \vec{\tau}_t = \sum_{t=1}^{t=4} (\vec{r}_t^{\,O} - \vec{r}_m^{\,O}) \times \boldsymbol{p}_t \cdot \vec{f}_t \quad (4)$$

Equation (5) defines the actual centre-of-mass $\vec{r}_m^{\,O}$ as function of its on-ground knowledge $\vec{r}_m^{\,\prime O}$ and its displacement $\overrightarrow{\delta r}_m^{\,O}$.

$$\vec{r}_m^{\,O} = \vec{r}_m^{\,\prime O} + \overrightarrow{\delta r}_m^{\,O} \quad (5)$$

Equation (6) defines the actual number of pulses per thruster $\boldsymbol{p}_t$ as function of its on-ground prediction $\boldsymbol{p}'_t$ and its difference $\boldsymbol{\delta p}_t$.

$$\boldsymbol{p}_t = \boldsymbol{p}'_t + \boldsymbol{\delta p}_t \quad (6)$$

Equation (7) can be obtained by combining equations (4), (5) and (6):

$$\overrightarrow{\delta r}_m^{\,O} \times \sum_{t=1}^{t=4} \boldsymbol{p}_t \cdot \vec{f}_t \approx \sum_{t=1}^{t=4} (\vec{r}_t^{\,O} - \vec{r}_m^{\,\prime O}) \times \boldsymbol{\delta p}_t \cdot \vec{f}_t \quad (7)$$

Equation (8) is equivalent to equation (7) where $\vec{\tau}_{unload}$ is the opposite of the perturbing torque that can be observed in the satellite telemetry:

$$\overrightarrow{\delta r}_m^{\,O} \times \sum_{t=1}^{t=4} \boldsymbol{p}_t \cdot \vec{f}_t \approx \vec{\tau}_{unload} \quad (8)$$

Displacements of the centre-of-mass can be estimated from equations (7) and (8). Both equations show similar results as $\boldsymbol{\delta p}_t$ and $\vec{\tau}_{unload}$.are correlated.

Table 5 reports the centre-of-mass displacements for each maneuver computed with equation (7).

man#	COM displacement	
	Ys (mm)	Zs (mm)
1	-30.5	13.3
2	-35.9	21.1
3	-27.7	11.8
4	-22.2	6.3
5	-27.2	13.9

Table 5. COM displacements

A systematic bias can be observed in the centre-of-mass, leading to the hypothesis of inaccuracy in the manufacturer data for the definition of the centre-of-mass.

Figure 6 show the centre-of-mass displacement as function of the orbit position relative to the canonical position of the solar array, i. e. the solar array rotation angle. The close to linear variations between maneuvers might be explained by an eccentric rotation of the solar array with respect to its centre-of-mass.

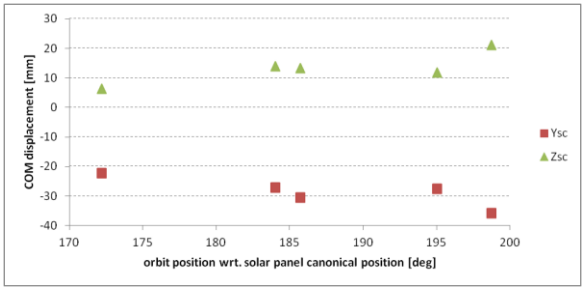

Fig. 6. Displacement of centre-of-mass as function of orbit position with respect to canonical position of the solar array

4. Reconstruction of the pulses distribution

Table 6 shows the differences in delta-v direction and maneuver duration if the average displacement computed in the previous section is applied to the centre-of-mass.

man#	delta-V difference [mm/s]			duration difference [%]
	radial	along-track	cross-track	
1	0.41	-0.79	0.01	-1.9
2	-1.57	0.22	-0.01	1.9
3	0.81	-1.11	0.01	-2.6
4	4.09	-2.51	0.03	-5.8
5	0.10	-0.63	0.00	0.2

Table 6. Maneuver reconstruction errors if average centre-of-mass displacement is considered

Table 7 shows the differences in delta-v direction and maneuver duration if linear evolution of the displacement of the centre-of-mass as function of the solar array rotation angle is applied.

man#	delta-V difference [mm/s]			duration difference [%]
	radial	along-track	cross-track	
1	0.57	-0.64	0.01	1.3
2	0.08	-0.84	0.00	-0.1
3	2.30	-2.15	0.02	1.6
4	0.09	-0.31	0.00	-3.1
5	-1.57	0.08	-0.01	-0.3

Table 7. Maneuver reconstruction errors if linear evolution of centre-of-mass displacement is considered

A clear improvement can be observed in both cases except in the case of the fourth maneuver.

5. Prediction of pulses distribution for OOP maneuver performed on 5th March 2017

Information from maneuvers 1 through 4 is used in the prediction of pulses distribution and its related consequences, delta-V direction and duration.

Table 8 shows the differences in delta-v direction and maneuver duration if average displacement is applied to the centre-of-mass.

man#	delta-V difference [mm/s]			duration difference [%]
	radial	along-track	cross-track	
5	-0.42	-0.97	0.00	0.8

Table 8. Prediction error for last OOP maneuver for average evolution

Table 9 shows the differences in delta-v direction and maneuver duration if linear evolution of the displacement of the centre-of-mass as function of the solar array rotation angle is applied.

man#	delta-V difference [mm/s]			duration difference [%]
	radial	along-track	cross-track	
5	-1.30	-0.48	-0.01	-0.3

Table 8. Prediction error for last OOP maneuver for linear evolution

A significant improvement is observed in both cases regarding the main thrust direction and maneuver duration mitigating the need of an early in-plane maneuver and allowing good performances in orbit determination process.

Figure 7 shows the residuals of the orbit determination process if no correction is applied to the maneuver duration. It can be seen that orbit determination process fails at calibrating the maneuver performances as it cannot model the induced change in the right ascension of ascending node.

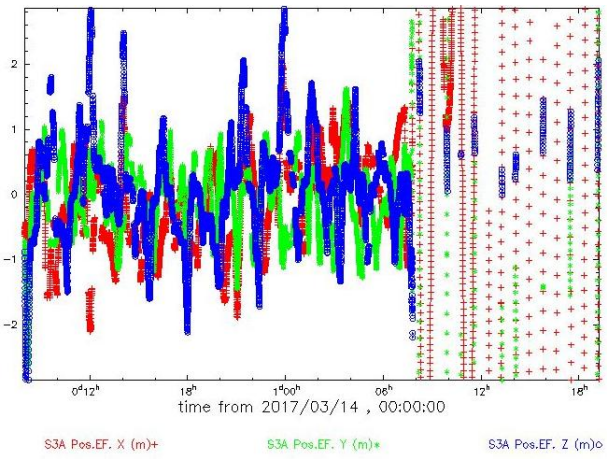

Fig. 7. Residuals of the orbit determination process with calibration of 15/03/2017 OOP maneuver with no correction applied to predicted duration

Figure 8 shows the residuals of the orbit determination process if correction based on Table 8 is applied to the maneuver duration. It can be seen that the orbit determination results improve significantly allowing a reasonably good solution.

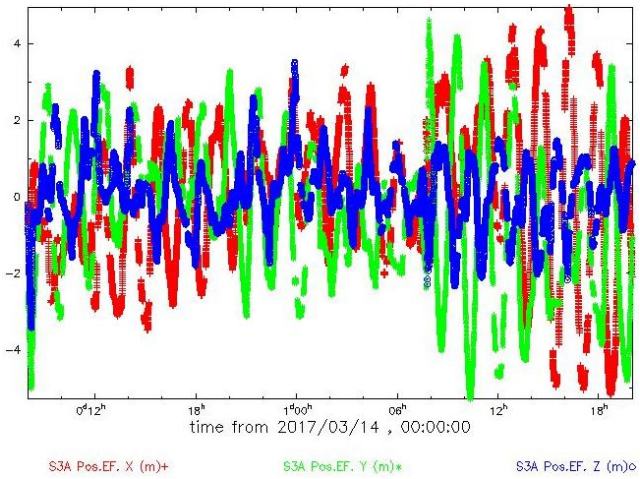

Fig. 8. Residuals of the orbit determination process with calibration of 15/03/2017 OOP with correction applied to predicted maneuver duration

6. Conclusions

Maneuver characteristics predictions can be improved by adjusting the satellite centre-of-mass based on information from previous maneuvers allowing reasonably good results in post-maneuver orbit determination process and reducing the risk of needing an early in-plane maneuver.

Data from future OOP maneuvers will help calibrating better the behavior of the maneuvers and hence their prediction.

References

1) Thales Sentinel-3 Flight Operations Manual, S3-MA-TAF-SC-01456
2) Thales Sentinel-3 Ground Procedure Specification for OCM Telecommand, S3-MO-TAF-01045